Görgün, E., Bohnhoff, M., Bulut, F., Dresen, G. (2010): Seismotectonic setting of the Karadere-Ducze branch of the North Anatolian Fault Zone between the 1999 Izmit and Ducze ruptures from analysis of Izmit aftershock focal mechanism. - Tectonophysics, 482, 1-4, 170-181,

DOI: 10.1016/j.tecto.2009.07.012

Seismotectonic setting of the Karadere-Düzce Branch of the North Anatolian Fault Zone between the 1999 Izmit and Düzce ruptures from Analysis of Izmit Aftershock Focal Mechanisms

Görgün, E., Bohnhoff, M., Bulut, F., Dresen, G.

Helmholtz Centre Potsdam GFZ, Telegrafenberg, 14473 Potsdam/Germany.

Contact: gorgun@gfz-potsdam.de

Ethem Görgün (corresponding author), e-mail: gorgun@gfz-potsdam.de, fax: 0049-3312881328

Marco Bohnhoff, e-mail: bohnhoff@gfz-potsdam.de, fax: 0049-3312881328

Fatih Bulut, e-mail: bulut@gfz-potsdam.de, fax: 0049-3312881328

Georg Dresen, e-mail: dre@gfz-potsdam.de, fax: 0049-3312881328

Abstract

We investigate aftershock focal mechanisms along the eastern part of the Izmit M_w = 7.4 August 17, 1999 rupture zone during the time period August 22, 1999 - October 17, 1999. Two spatial clusters of aftershock activity are analyzed representing the Karadere Fault (KF) and the Düzce Area (DA). Based on an aftershock hypocenter catalogue restricted to events with horizontal and vertical errors < 2 km, we determine fault plane solutions for 221 events. The high number of focal mechanisms at the eastern Izmit rupture zone could be determined only due to the low magnitude-detection threshold of the seismic network and allows to resolve the local deformation pattern with unprecedented precision. Focal mechanisms along the Karadere Fault allow us to identify dominantly dextral strike-slip mechanisms with normal faulting components on NE-SW trending fault planes. Focal mechanisms in the Düzce Area predominantly exhibit NE-SW extensional normal faulting but also a substantial part of strike-slip faulting. Further subdivision of the data set slightly decreases for the misfit for deeper (z > 10 km) events. At the junction between the Karadere and Düzce Faults, where the North Anatolian Fault Zone (NAFZ) strike is bending from 65° to 90° (EW) at the eastern end of the Izmit rupture we observe a high variance in stress field orientation. High variance northeast of Karadere Fault correlates with lower *b*-values. While the Karadere Fault reflects a predominant dextral strike-slip regime with normal faulting components, the Düzce Area further to the East that also hosted the forthcoming M_w 7.2 mainshock 87 days after the Izmit earthquake can be subdivided into a dominantly NE-SW extensional normal faulting regime below the Düzce Basin (DB) and a first-order strike-slip regime along the western Düzce Fault (DF). We conclude that the Düzce Basin was set under tension by

the Izmit rupture and partly released the slip deficit by extensional faulting on Karadere Fault parallel to the coseismic displacement. At the same time this area and in particular the Düzce Fault that bounds the Düzce Basin to the south reflects mostly strike-slip events representing a major asperity along the NAFZ before initiating the Düzce rupture 87 days after the Izmit event.

Key words: North Anatolian Fault Zone, Izmit earthquake, Fault plane solutions, Stress tensor inversion, seismotectonics.

1. Introduction

The North Anatolian Fault Zone (NAFZ) is one of the seismically most active transform faults worldwide extending along 1600 km from eastern Anatolia to the Aegean Sea (Figure 1a). The direction of slip corresponds well with the Global Positioning System (GPS) derived 25-30 mm yr^{-1} westward motion of the Anatolian Block with respect to Eurasia (McClusky et al., 2000; Reilinger et al., 2006). The M_w = 7.4 August 17, 1999 Izmit earthquake exhibits a maximum surface displacement of > 5 m at the Sapanca-Akyazi segment (Barka et al., 2002, Figure 1b). Average coseismic slip obtained from teleseismic waveform inversion is 2.5 m (Tibi et al., 2001) and 2.9 m from regional strong-motion records (Bouchon et al., 2002). Moreover, Synthetic Aperture Radar interferometry (InSAR) data inversion (Wright et al., 2001) and GPS data by Reilinger et al. (2000) show a maximum displacement of 5 m and 3.5 m near the mainshock epicenter, respectively. Delouis et al. (2002) identified four individual segments along the Izmit rupture by using combined GPS, SAR, teleseismic and strong-motion data.

Rupture propagation towards the east ended near Düzce where a large earthquake occurred 87 days after the Izmit event (November 12, 1999 M_w = 7.2). Fault plane solutions of both mainshocks reflect right-lateral strike-slip faulting on vertical (Izmit) and steeply northward dipping (Düzce) fault plane (Tibi et al., 2001, see Figure 1b). The easternmost segment of the 1999 Izmit earthquake rupture is right stepping at the Karadere area (1.5 m of co-seismic slip) with respect to the Düzce Area (no co-seismic slip at the surface). Izmit aftershock focal mechanisms for this area for magnitudes > 2

based on recordings from the combined German Task Force (GTF) and SApanca BOlu NETwork (SABONET) are predominantly strike-slip with normal faulting components (Bohnhoff et al., 2006).

The apparent dissimilarity between aftershock mechanisms is so strong that it suggests a post-earthquake stress field with little resemblance to stresses release in the mainshock. The local stress field is not mainly controlled by the rupture characteristics of the mainshock (Michael et al., 1990: Michael 1991).

In this study we determine and analyze a total of 221 Izmit aftershock focal mechanisms for the Karadere-Düzce branch for the entire recording period of the seismic network (August 22, 1999 - October 17, 1999) and down to M_l = 0.9. We perform stress tensor inversion to determine the local stress field orientation. Results are compared to the local tectonic setting and discussed in the light of the proceeding Düzce earthquake that occurred on November 12, 1999 extending the Izmit rupture by ~50 km to the east.

2. Data base and procedure

We focus on recordings obtained by a 36-seismic station network covering the entire Izmit rupture zone extending from the eastern Sea of Marmara towards the Düzce Area. A long-term seismic network consisting of 15 stations was in operation since 1996 (SApanca-BOlu NETwork - SABONET, Milkereit et al., 2000, yellow triangles in Fig. 1b). With the aim to monitor the Izmit aftershock activity at low magnitude-detection threshold, the German Task Force for Earthquakes (GTF) of the Helmholtz-Centre Potsdam - GFZ deployed additional 21 stations (Figure 1b, red triangles) in the area

within the first four days after the mainshock (Zschau and Grosser, pers. comm.). The hypocenter catalog derived from the combined network consists of 10066 hypocenters that show distinct spatial clustering along the rupture (Bohnhoff et al., 2007; Bulut et al., 2007).

With the aim to further analyze the seismotectonic setting after the Izmit event and prior to the Düzce event we focus on the eastern Izmit rupture zone in the Karadere-Düzce Area (Figure 1b). There, the Izmit rupture terminated at depth of the intersection between the Karadere and Düzce Faults where the NAFZ bends by ~25°. We select all events in that area that have at least 10 P onset picks at good azimuthal coverage (maximum gap < 110°). This resulted in a total of 353 events that cover a magnitude range from $0.9 < M_l < 4.3$. We use relocated hypocenters that were determined based on applying the double-difference technique resulting in a relative location accuracy of ~400 m (see Bulut et al., 2007 for details). Using P polarities we apply the FOCMEC program (Snoke, 2003) that performs a grid-search assuming a pure double-couple mechanism. At least 10 P-wave first-motion polarities with a maximum gap of 110° are used to determine fault plane solutions and only events with errors < 10° for strike, dip and rake were considered for further analysis. A total of 211 events fulfilled the error quality test for the area of investigation. Error bounds for the 211 obtained fault plane solutions are plotted in Figure 2 in terms of errors for strike, dip and rake, respectively. Averages of P-wave polarity and azimuthal gap are 15 and 92°, respectively. In addition, we include fault mechanisms for this area as determined from earlier studies including events from the first week after the mainshock (Bohnhoff et al., 2006) resulting in a total of 221 fault plane solutions.

Figure 3a shows the entire set of fault plane solutions in a lower hemisphere equal-area/angle projection. Predominant activity is observed throughout the Düzce Area (DA) in more cloud-type distribution and along the Karadere Fault (KF) that strikes 65° and that dips at ~80° to the NW. In Figure 3b we plotted all epicenters shown in Figure 3a and added the focal mechanisms of the three largest aftershocks (M_l > 4) that all occurred during the first hours of the mainshock, the Izmit subevent S1 that represent the last part of the segmented Izmit rupture (M_w = 6.9, see Tibi et al., 2001) and the Düzce mainshock (M_w = 7.2). Interestingly, all these events have an almost identical focal mechanism indicating right-lateral slip on a steeply northward dipping, EW-trending fault below the southern part of the Düzce Basin. For further analysis we focus on the orientations of the axes of maximum compression (P) and tension (T) in the following. In Figure 4a-d we show four events that are representative for the entire set of fault mechanisms. The events shown in Figure 4a (15 P-wave first-motion polarities, 104° azimuthal gap), 4c (10 P-wave first-motion polarities, 109° azimuthal gap) are examples of strike-slip fault plane solutions along Karadere and Düzce Faults. The focal mechanisms shown in Figure 4b (13 P-wave first-motion polarities, 96° azimuthal gap), 4d (12 P-wave first-motion polarities, 71° azimuthal gap) are examples for normal faulting mainly in the Düzce Basin. In Figure 5a and 5b we plot the P and T axes of the entire catalogue of focal mechanisms in an equal-area/angle projection of the lower hemisphere and scale the size and shading of circles with magnitude and time, respectively. While P axes form a great circle trending NNW-SSE the T axes cluster at low dip angle trending NE-SW. Dominantly strike-slip and normal faulting mechanisms are observed for the events of the data set.

To further analyze the data set for spatial clustering of similar faulting mechanisms we proceed as follows: As a first step the Karadere-Düzce area is divided into the Karadere Fault (KF) and Düzce Area (DA) (see Figure 3a) containing 56 and 165 events, respectively. This subdivision is based on structural information of the area and spatial clustering of hypocenters that allow defining a steep NE-SW trending plane of activity along the Karadere Fault and a diffuse cloud-type activity in the Düzce Area. Note that this difference in hypocentral distribution is real and not an artifact of varying location precision with the area (Bulut et al., 2007).The Düzce Area was then further subdivided into a northern part covering the Düzce Basin (DB) and a southern part along the Düzce Fault (DF) (Figure 3b).

The Düzce Area (DA) contains 165 fault plane solutions at depths between 2 and 16 km and at a magnitude range between 0.9 and 4.3. The fault mechanisms within DA reflect a predominant NW-SE extensional normal faulting mechanism and some are right-lateral strike-slip mechanisms (Figure 6a). The Karadere Fault (KF) covers the area surrounding the Karadere Fault and contains 56 events. These occurred at depths between 10.5 and 15 km and reflect the down-dip extension of the surface trace of the KF. The event magnitudes are between 1.2 and 3.5. The distribution of P and T axes indicates a dominantly strike-slip mechanism with normal faulting components. The P axes reflect a scattered orientation with an average NW-SE trend and the T axes are found to cluster at a subhorizontal NE-SW trend (Figure 6b).

In the northern DA (Düzce Basin) there are 96 fault plane solutions and the P and T axes reflect dominantly normal faulting. The P axes show NW-SE orientation and the T axes display a scattered orientation with an average NE-SW trend (Figure 6c). The

southern zone of DA (Düzce Fault) contains 69 aftershock fault mechanisms. The P axes are trending NNW-SSE at various dip angles and the T axes are trending NE-SW at shallow dip angles. Therefore, this area reflects both strike-slip and normal faulting mechanisms (Figure 6d).

In a second step, we subdivide the Düzce Area data set according to event magnitude (M > 2, 53 events, and M < 2, 112 events) and depth (z > 10 km, 104 events and z < 10 km, 61 events). In the following each of the subsets introduced above is inverted to determine the directions of the principal stresses and the relative stress magnitude.

3. Stress tensor inversion

Numerous methods have been proposed for the determination of the stress field orientation from fault plane solutions. The most widely used ones are the inversion algorithms of Gephart and Forsyth (1984) and Michael (1984). Both methods are based on the assumption that, if various orientations of focal mechanisms exist within a region of uniform stress, one may determine the directions of the principles stresses ($\sigma_{1\text{-}3}$) and a relative stress magnitude (Φ) from the condition that slip occurs in the direction of maximum shear stress. The main difference between these methods is the description of the deduced misfit and the way to define the best model. The reliability of the deduced stress field orientation (misfit value and variance) reflects the level of stress field heterogeneity (Gephart, 1990; Michael 1987, 1991; Bohnhoff et al., 2004).

Hardebeck and Hauksson (2001) performed an extensive comparison of both methods based on synthetic focal mechanism data sets. The accuracy with which both inversion methods determine stress parameters were found to be generally good. The accuracy of both methods improves with increasing size of data sets, with the most improvement occurring between $N = 20$ and $N = 50$ (Hardebeck and Hauksson, 2001).

In our study we applied the technique of Michael (1984; 1987) to the catalogue as a whole as well as to the individual subsets as described above. The method of Michael (1984; 1987) provides a more appropriate estimate of uncertainty (Hardebeck and Hauksson, 2001). The algorithm uses the statistical method of bootstrap resampling and allows determining the orientation of the three principles stresses (σ_1 = maximum principal compressive stress, σ_2 = intermediate and σ_3 = minimum) as well as a relative stress magnitude $\Phi = (\sigma_2 - \sigma_3)/(\sigma_1 - \sigma_3)$ (Bott, 1959). The stress magnitude is defined using the standard geologic/geophysical notation with compressive stress positive and $\sigma_1 > \sigma_2 > \sigma_3$, so that σ_1 is the maximum and σ_3 the minimum principal compressive stress (Zoback, 1992). These parameters are determined by finding the best fitting stress tensor to the observed focal mechanisms. Assumptions that need to be fulfilled by the input data are: (1) stress is uniform in the area of investigation during the observed time interval, (2) the earthquakes are shear-dislocations on pre-existing faults, (3) similar shear stress magnitude are present on each fault (specific for Michael routine) and (4) slip occurs in the direction of the resolved shear stress on the fault plane.

To quantify the misfit between the best stress tensor and the data, the angle between calculated slip vector from stress tensor inversion and observed slip vector from fault plane solutions is used. This angle is referred to as β, and the angle $\overline{\beta}$ refers to the

mean β for the data in a single inversion (Michael, 1987). A synthetic control study also showed that the amount of heterogeneity in the stress field could be characterized by the average misfit ($\overline{\beta}$) between the observed and predicted slip directions (Michael et al., 1990). For focal mechanism data with errors of < 10°, $\overline{\beta} \approx 33°$ when the spatially uniform and variable parts of the stress field have equal size (Michael, 1991). If $\overline{\beta} > 33°$, we will interpret the inversion results to imply a spatially heterogeneous state of stress. We start to invert the entire data set for the stress tensor followed by independent inversions for various subsets in order to detect variations of the local stress field.

4. Results

In order to determine the stress field orientation at the Karadere-Düzce segment of the NAFZ from the fault mechanism data we started by inverting the entire set of 221 fault plane solutions (Figure 7). A vertical orientation (plunge of 84°) is found for the maximum principal stress, σ_1. The minimum principal stress, σ_3, is found to be subhorizontal striking NE-SW. The intermediate principal stress, σ_2, is subhorizontal trending NW-SE. The confidence intervals of σ_1 and σ_2 are strongly clustered around the stress axes indicating a stable normal faulting stress regime. However, substantial heterogeneity is observed due to the large misfit of $\overline{\beta} = 58°$. According to Michael (1991), we can state that the stress field is heterogeneous and does not show the actual result, the acceptable level of $\overline{\beta}$ should be $\leq 33°$ if errors of fault plane solutions are < 10° for strike, dip and rake angles. Heterogeneity of the stress field is reflected by the average misfit level of the inversion. For each stress inversion, 2000 bootstrap iterations

were performed. In order to further resolve the source of stress field heterogeneity, subsets of the fault plane data are formed based on the inferred extent of the mainshock rupture, structural variations within the area of investigation, and the relocated aftershock hypocenters as discussed in the previous section. Results of the individual inversions are given in Table 1. Inverting the subsets for the Karadere Fault (KF) and the Düzce Area (DA) result in a significantly decreased misfit of 30° for KF. However the misfit of DA (54°) can be hardly reduced. A clear NE-SW extensional normal faulting regime is found for the Düzce Area with an almost vertical orientation for σ_1 (plunge 84°) (Figure 8a). The results are thus very similar to that found for the entire data base which is well explained by the large number of events that dominate the whole data set. The relative stress magnitude for the Düzce Area is 0.5 indicating that the magnitude of σ_2 is equal to $\frac{\sigma_1 + \sigma_3}{2}$. In contrast, a strike-slip regime with notable normal faulting component is observed for the Karadere Fault (σ_1 trend N133°E, plunge 19°, σ_2 trend N38°W, plunge 70°) (Figure 8b). The relative stress magnitude is estimated to be ~0.8 for the Karadere Fault. The confidence intervals for σ_1 and σ_2 strike in NW-SE direction and almost overlap. These results confirm that two separate stress field orientations exist in the broader Karadere and Düzce area.

Inversion of the remaining subsets DB and DF reveal that both segments separately reflect a substantial higher level of uniform stress with $\overline{\beta}$ =32° and $\overline{\beta}$ = 30°, respectively. A NE-SW extensional normal faulting regime is observed below the Düzce Basin (Figure 8c). Instead, the Düzce Fault shows a strike-slip stress regime with normal faulting components; σ_1 is subhorizontal and trends N151°E (Figure 8d). The stress field at the Düzce Fault is thus similar to that identified at the Karadere Fault but rotated ~20°

clockwise. The Düzce Fault may be the main active branch of the NAFZ forming the southern boundary of the NE-SW extending Düzce Basin.

We subdivide the DA data set into large ($M_l > 2$) and small ($M_l < 2$) events to look for scale-dependent variations of the stress field. We observe no first-order variation for $\sigma_{1\text{-}3}$ and only minor differences in the size of confidence intervals (Figure 9a-b).

Looking for depth-dependent changes we subdivide the data at DA after hypocentral depth. Stress tensor inversion results for z > 10 km (104 fault plane solutions) and z < 10 km (61 fault plane solutions) are shown in Figure 9c and 9d, respectively. At > 10 km depth the stress field is purely NNE-SSW extensional whereas it reflects NE-SW extensional normal faulting regime with a strike-slip component at shallow depth.

As we observe a dramatic decrease in $\overline{\beta}$ value with respect to DA in case the fault plane solution catalogue is divided into the subsets, it has to be checked whether this observation has a physical meaning. We experiment with randomly defined subsets of DA for which the number of inputs as well as spacing of events in regional scale is similar to the scale-dependent analysis (number of fault planes is for example 55 and 91). Stress tensor inversion results from the randomly created subsets show that $\overline{\beta}$ values do not depend on decrease in number of inputs (in Figure 10).

To search entire data set (221 fault plane solutions) for spatial variations of the stress field we apply the relevant part of the software package ZMAP (Wiemer, 2001). We apply Michael's inversion algorithm to measure heterogeneity and misfit along the Karadere-Düzce Area (KDA). High variance, or high misfit, indicates a poor fit of a homogeneous stress tensor to the observed focal mechanism, and shows high

heterogeneity of the stress field (Michael et al., 1990; Lu et al., 1997; Wiemer et al., 2002). The results from the stress tensor inversions based on subvolumes with a radius of 1 km in horizontal direction and no depth limitation containing at least 12 focal mechanisms are shown in map view in Figure 11a. The direction of the maximum principle stress (σ_1) from the stress tensor inversion result is plotted on KDA of the NAFZ (Figure 11a). This is expected from the derived local stress fields as described above. A systematic change from a strike-slip regime at the Karadere and western Düzce Faults towards an extensional regime below the Düzce Basin and eastern DF is observed in more detail from Figure 11a. Note, that the Düzce Fault was active after the Izmit event and prior to the Düzce event only at the western part close to the bending point of the NAFZ (at the intersection between the Karadere and Düzce Faults) [Bohnhoff et al., 2007]. The Düzce Fault towards the east south of the Düzce Basin was only activated during the Düzce mainshock and thus is not sampled based on the Izmit aftershocks used in this study. The variance of the resulting stress tensor at each subvolume is calculated and shown color coded in Figure 11b. The highest values for the variance (> 0.2) are found near the junction of the Karadere and Düzce Faults where the NAFZ has its bending point from 65° to EW.

We compare our stress tensor inversion results with Bohnhoff et al. (2006) for DF. Bohnhoff et al. (2006) found a strike-slip regime with a relative stress magnitude of Φ = 0.63. The maximum principle stress is subhorizontal and trends N159°E. In this study we further decreased the magnitude threshold for fault plane solutions allowing to substantially increase the number of events to be inverted for the stress tensor. We almost obtain similar results for σ_1 (N151°E) and Φ (0.7) at DF.

5. Discussion

The 1999 Izmit and Düzce mainshocks reflect a clear E-W trending right-lateral strike slip faulting mechanism which is in good agreement with the regional tectonic setting along the NAFZ as a first order approximation (Tibi et al., 2001). Similar results for fault kinematics and local stress field orientations were found earlier for KDA based on the analysis of larger magnitude faulting mechanisms (Örgülü et al., 2001; Bohnhoff et al., 2006). A regional right-lateral strike-slip regime dominates reflecting the > 25-30 mm yr^{-1} westward migration of Anatolia with respect to stable Eurasia (McClusky et al., 2000; Flerit et al., 2004; Reilinger et al., 2006). However, on the local scale the NAFZ consists of branches where the fault trends and the local stress regime systematically vary as shown e.g. for the Çınarcık and Akyazi areas (Bohnhoff et al., 2006).

Areas with high coseismic slip show aftershocks that are dominantly strike-slip, but low slip barriers show mostly normal faulting aftershocks. A previous stress field analysis based on stress tensor inversion shows a clear stress partitioning and rotations of the local stress field following the Izmit mainshock (Bohnhoff et al., 2006). In this study we determine a total of 221 Izmit aftershock focal mechanisms including also the smaller ($M < 2$) events and using the entire recording period of the seismic network.

The transition between the Karadere Fault and the Düzce Area is located exactly where the Izmit rupture terminated towards the east. The Düzce Basin itself shows dominantly normal faulting. Interestingly, the Düzce mainshock reflects dominantly strike-slip faulting on a steeply northward dipping EW-trending fault plane. It is noted

that the larger (M_l > 4) Izmit aftershock fault mechanisms in the Düzce Area all occurred during the first hours after the mainshock reflecting a similar mechanism as the Düzce mainshock (Figure 3b). Furthermore, a subevent of the Izmit mainshock identified in this area by Tibi et al. (2001) also reflects the same mechanism. The structure highlighted by all these events during the small time window right after the Izmit mainshock probably represents the southern border fault of the Düzce Basin. The Izmit rupture included ~1.5 m right-lateral surface slip on the Karadere Fault but none in the Düzce Area. Our results indicate that the Düzce Basin was set under tension by the Izmit mainshock resulting in normal faulting within the Basin and strike-slip on the vertical Düzce Fault representing the main branch of the NAFZ in this area. However, it was only 87 days later that the whole Düzce segment was activated extending the rupture by ~50 km to the east. Figure 11a shows the distribution of the faulting types for the entire Karadere-Düzce area. Bars display the orientation of the maximum principle stress (σ_1) with regard to different faulting regimes. It is noted that there are two different faulting types, strike-slip and normal faulting, between the southern and northern Düzce areas, respectively. The focal mechanisms along the Karadere Fault reveal dominantly right-lateral strike-slip motion but also a contribution from normal faulting.

The focal mechanisms analyzed in this study have errors < 10° and high confidence levels as they were determined from a local seismic network with good azimuthal coverage. The resulting $\overline{\beta} \leq 33°$ for the individual areas is acceptable to propose a rather homogeneous and uniform stress field in the different areas (Karadere Fault, Düzce Fault, Düzce Basin) (Michael, 1991). The subsets for magnitudes > 2.0 and depths > 10 km give slightly smaller misfit than the subsets for magnitudes < 2.0 and

depths < 10 km but highly similar stress field orientations in general. The volumes have small enough misfit values to satisfy our criterion for relatively homogeneous data sets but do not hint towards a first-order dependence of the stress field homogeneity on the size of the rupture planes or the confining pressure down to ~16 km depth.

Mapping out the variance of the best fitting stress tensors we find the highest values north of the 65° striking Karadere Fault and the EW-striking Düzce Fault (Figure 11b). The variance of the stress field is also high close to the location of the Düzce mainshock. High variance or high misfit indicates a poor fit of a homogeneous stress tensor to the observed focal mechanism and therefore indicates high heterogeneity of the stress field (Michael et al., 1990; Gillard et al., 1996; Lu et al., 1997; Wiemer et al., 2002).

Seeber et al. (2000) observed that the focal mechanisms of aftershocks in this area are highly diverse, pointing to a strongly heterogeneous stress field that may have been partially created during the ruptures of the Izmit mainshock. Such a heterogeneous stress field may be responsible for generating or activating complex sets of fractures in the material off the mainshock rupture zones, so-called secondary faults. The average fast polarization directions from ray paths that propagate inside the Almacik block, south of the Karadere–Düzce area, are neither parallel to the local fault strike nor to the expected regional maximum compressive stress direction. The large overall spatial variations of the results imply that multiple structures and mechanisms contribute to the observed crustal anisotropy in this area (Peng and Ben-Zion, 2004).

Wiemer et al. (2002) proposed a heterogeneous stress field hypothesis. The mainshock causes a redistribution of stress in its immediate vicinity. It is reasonable to

assume that the stress will be significantly modified, and overall reduced, near the rupture zone. The complex slip distribution during the mainshock causes a heterogeneous stress re-distribution at and near the activated fault segment. Consequently, this produces locally varying focal mechanisms and, in part, a high variance of the stress field. This high degree of heterogeneity in stress also causes high *b*-values, since numerous small faults in multiple orientations can be activated. Here the resulting stress field is observed to be more heterogeneous (> 0.2) [Figure 11b] with the mean aftershock magnitude larger (low *b*-value) at the KF/DB junction. The Izmit rupture is ended here and does not continue further east. However, low *b*-values are correlated with smaller variance (< 0.2) in east of DB and DF (Figure 11b and 12). In this study a heterogeneous stress field hypothesis for Wiemer et al. (2002) does not correspond in the KF/DB junction. We currently cannot offer an explanation why low *b*-values are correlated with high variance for this area. This may either be connected with the rupture dynamics, or pre-existing features of the crust.

The predominant orientation of the Karadere Fault was identified to be N65°E extending for about 25 km along strike dipping with ~67° to the north. This area hosted ~1.5 m of right-lateral coseismic slip during the Izmit mainshock. It is noted that 53 fault mechanisms are analyzed as determined for the former study (Bohnhoff et al., 2006) at the Karadere-Düzce area. Based on 53 fault plane solutions the analysis of stress orientation and fault mechanisms for this area indicate mainly strike-slip. The maximum principle stress (σ_1) is subhorizontal and trends N159°E, indicating a clockwise rotation of > 30° with respect to the regional stress field (see also Bohnhoff et al., 2006). In this study the number of Izmit aftershock focal mechanisms was substantially increased

allowing to further subdivide the Karadere Fault segment and allowing to identify local variations of the stress field orientation. Right-lateral strike slip faulting is found at the Karadere Fault. Events with magnitudes ranging from 1.2 to 3.5 are located at 10.5-15 km depths at the down-dip extension of the surface trace of the fault (Bulut et al., 2007). For the Karadere segment of the NAFZ the orientation of σ_1 is N133°E with a plunge of 19°.

There was no surface rupture observed along DF after the Izmit earthquake, thus the Izmit rupture was ended at the end of the KF (Barka et al., 2002). The easternmost segment of the Izmit earthquake ruptured a small part of the east-west trending fault bounding the Düzce pull-apart basin in the south (the Düzce Fault). The slip along this fault associated with the Izmit earthquake is small (several centimeters) and apparently vanishes eastward. It is remarkable that the surface rupture associated with the Düzce earthquake follows the southern boundary fault of the Düzce Basin, rebreaks the last segment of the Izmit earthquake, and creates significant new rupture along the eastern part of the fault (Aydin and Kalafat, 2002; Duman et al., 2005; Pucci et al., 2006) [Figure 12]. Obviously, the 87 days between the Izmit and Düzce earthquakes point out the time dependence of the failure event.

The hypocenter catalog of Izmit aftershocks indicates a sharp termination of activity towards the eastern end of the rupture where the Düzce earthquake initiated 87 days later (Bohnhoff et al., 2007; Bulut et al., 2007). This boundary correlates with high *b*-values (Görgün et al., subm.) (Figure 12). Afterslip apparently extended east of the eastern end of the rupture (Karadere segment), which possibly helped to trigger 12 November 1999 M_w Düzce earthquake that extended the Izmit rupture about 40 km

further east (Reilinger et al., 2000). The Düzce mainshock initiated its rupture below the Düzce Basin, probably on the down-dip extension of the Düzce Fault. Evaluating seismological data that were collected from strong motion and teleseismic records suggested 64° N for the dip angle of the Düzce mainshock (Umutlu et al., 2004). The Düzce epicenter is located ~5 km north of the Düzce Fault (Figure 12). This epicentral offset from the Düzce Fault depends on the dip (64° N) and strike (264°) angles, and hypocentral depth (12.5 km) of the Düzce mainshock. Evaluating seismological data that were collected from SABONET suggests about 66° N for the dip angle of the Düzce rupture (Milkereit et. al, 2000). The rupture propagated to the east along the Düzce Fault and also to the west, partly re-rupturing the westernmost Düzce Fault (Umutlu et al., 2004). The maximum principle stress directions in this study indicate a subvertical NW-SE trend at the Düzce Basin. The eastern rim of the Izmit aftershock activity indicates that the Izmit earthquake already ruptured parts of the Düzce Fault segment (Figure 12). Comparing the location of the Izmit aftershocks at the eastern end of the rupture with the observed surface rupture of the Düzce earthquake, it is apparent that half of the Düzce rupture trace was seismically active already after the Izmit earthquake. The slip deficit between the Karadere Fault (1.5 m) and the Düzce Fault (0 m) has set the Düzce Basin under tension producing NE-SW extensional normal faulting aftershocks at the eastern end of the Izmit rupture and contributing to activate the Düzce Fault that acted as an asperity prior to the Düzce mainshock.

Aftershock fault plane solutions in the Karadere Fault are mainly related to combined right-lateral strike-slip and normal faulting with a NW-SE orientation for the maximum principle stress (N133°E trend, 19° plunge). The Düzce Basin is related to a

clear NE-SW extensional normal faulting regime indicating a pull-apart structure with an almost vertical orientation (84° plunge) for the maximum principal stress.

6. Conclusions

Fault plane solutions for Izmit aftershocks along the Karadere-Düzce section of the Izmit rupture are analyzed to determine the deformation and stress regimes. Fault mechanisms for aftershocks recorded by German Task Force and Sapanca Bolu Network are used. 221 highly reliable fault plane solutions are determined from Izmit aftershocks along the eastern part of the rupture (Karadere-Düzce branch) covering a magnitude range between 0.9 and 4.3, during the time span between 22 August and 17 October 1999. Stress tensor inversion of the data allows to identify two separate predominant stress regimes. While strike-slip dominates along the Karadere and Düzce Faults we observe a NE-SW extensional normal faulting regime below the Düzce Basin that is bounded to the south by the Düzce Fault. The high number of focal mechanisms could be determined only due to a dense seismic network recording aftershock activity at low magnitude-detection threshold allowing to resolve variations in the stress field along the eastern part of the Izmit rupture. At the junction between the Karadere and Düzce Faults, where the North Anatolian Fault Zone strike is bending from 65° to 90° (EW) at the eastern end of the Izmit rupture we observe a high variance in stress field orientation. High variance northeast of Karadere Fault correlates with lower *b*-values. We conclude that the Düzce Basin was set under tension by the Izmit mainshock and represents a pull-apart structure similar to the Akyazi Plain further to the west. The Düzce Fault was

activated in part towards the end of the Izmit rupture but did not rupture entirely until 87 days later although producing dominantly strike-slip events along its western part. This part of the NAFZ is therefore interpreted as a classical example of a fault asperity.

Acknowledgements

We thank the German Task Force for Earthquakes (GTF) hosted at Helmholtz Centre Potsdam GFZ and especially Jochen Zschau and Helmut Grosser for providing the continuous seismic recordings obtained by the GTF network after the 1999 Izmit earthquake. We thank Erwin Günther, Sami Zünbül and Salih Karakisa for maintenance of the network. Furthermore we thank Grzegorz Kwiatek and Katrin Plenkers for constructive discussions and, Dino Bindi and Stefano Parolai for support during magnitude determination. Some figures were generated by the Generic Mapping Tools (GMT) code developed by Wessel and Smith (1991). We also thank Oliver Heidbach (the managing editor), Andrew J. Michael and an anonymous reviewer for their constructive comments and suggestions which improved the manuscript.

References

Aydin, A. and Kalafat, D., 2002. Surface Ruptures of the 17 August and 12 November 1999 Izmit and Düzce Earthquakes in Northwestern Anatolia, Turkey: Their Tectonic and Kinematic Significance and the Associated Damage, Bull. Seism. Soc. Am., 92(1), 95-106.

Barka, A., Akyüz, H. S., Altunel, E., Sunal, G., Çakir, Z., Dikbas, A., Yerli, B., Armijo, R., Meyer, B., Chabalier, J. B. de, Rockwell, T., Dolan J. R., Hartleb, R., Dawson, T., Christofferson, S., Tucker, A., Fumal, T., Langridge, R., Stenner, H., Lettis, W., Bachhuber, J. and Page, W., 2002. The Surface Rupture and Slip Distribution of the 17 August 1999 Izmit Earthquake (M 7.4, North Anatolian Fault, Bull. Seism. Soc. Am., 92(1), 43-60.

Bohnhoff, M., Baisch, S.&Harjes, H.-P., 2004. Fault mechanisms of induced seismicity at the superdeep German Continental Deep Drilling Program (KTB) borehole and their relation to fault structure and stress field, J. Geophys. Res., 109, B02309, doi: 10.1029/2003JB002528.

Bohnhoff, M., Grosser, H. and Dresen, G., 2006. Strain Partitioning and Stress Rotation at the North Anatolian Fault Zone from aftershock focal mechanisms of the 1999 Izmit Mw=7.4 Earthquake, Geophys. J. Int., 166, 373–385.

Bohnhoff M., Bulut, F., Görgün, E., Milkereit, C., Dresen, G., 2007. Seismotectonic setting at the North Anatolian Fault Zone after the 1999 Mw=7.4 Izmit earthquake based on high-resolution aftershock locations, Adv. Geosci., 14, 1-8.

Bott, M. H. P., 1959. The mechanics of oblique slip faulting, Geol. Mag., 96, 109-117.

Bouchon, M., Töksöz, M. N., Karabulut, H., Bouin, M. P., Dietrich, M., Aktar, M. & Edie, M., 2002. Space and Time Evolution of Rupture and faulting during the 1999 Izmit (Turkey) Earthquake, Bull. Seism. Soc. Am., 92(1), 256-266.

Bulut, F., Bohnhoff, M., Aktar, M., Dresen, G., 2007. Characterization of aftershock-fault plane orientations of the 1999 Izmit (Turkey) earthquake using high-resolution aftershock locations, Geophys. Res. Lett., Vol. 34, L20306, doi: 10.1029/2007GL031154.

Delouis, B., Giardini, C., Lundgren, P., and Salichon, J., 2002. Joint inversion of InSAR, GPS, Teleseismic and Strong-Motion Data for the Spatial and Temporal Distribution of Earthquake slip: Application to the 1999 Izmit Mainshock, Bull. Seism. Soc. Am., 92(1), 278-299.

Duman, Y.T., Emre, O., Dogan, A. and Ozalp, S., 2005. Step-over and Band Structures along the 1999 Duzce Earthquake Surface Rupture, North Anatolian Fault, Turkey, Bull. Seism. Soc. Am., 95(4), 1250-1262.

Flerit, F., Armijo, R., King, G. & Meyer, B., 2004. The mechanical interaction between the propagating North Anatolian Fault and the back-arc extension in the Aegean, EPSL, 224, 347–362.

Gephart, J.W., 1990. Stress and the direction of slip on fault planes, Tectonics, 9, 845–858.

Gephart, J.W. & Forsyth, D.W., 1984. An improved Method for Determining the Regional Stress Tensor Using Earthquake Focal Mechanism Data: Application to the San Fernando Earthquake Sequence, J. Geophys. Res., 89, 9305–9320.

Gillard, D., Wyss, M. and Okubo, P., 1996. Type of faulting and orientation of stress and strain as a function of space and time in Kilauea's south flank, Hawaii, Journal of Geophysical Research, 101, 16025-16042.

Görgün, E., Zang, A., Bohnhoff, M., Milkereit, C., Dresen, G., Analysis of Izmit aftershocks 25 days before the November 12th 1999 Düzce earthquake, Turkey, submitted to Tectonophysics, 2009.

Hardebeck, J. L. and Hauksson, E., 2001. Stress orientations obtained from earthquake focal mechanisms: what are appropriate uncertainty estimates? Bull. Seism. Soc. Am. 97, 826–842.

Lu, Z., Wyss, M. and Pulpan, H., 1997. Details of stress directions in the Alaska subduction zone from fault plane solutions, Journal of Geophysical Research, 102, 5385-5402.

McClusky, S., Balassanian, S., Barka, A., Demir, C., Ergintav, S., Georgiev, I., Gurkan, O., Hamburger, M., Hurst, K., Kahle, H., Kastens, K., Kekelidze, G., King, R., Kotzev, V., Lenk, O., Mahmoud, S., Mishin, A., Nadariya, M., Ouzounis, A., Paradissis, D., Peter, Y., Prilepin, M., Reilinger, R., Sanli, I., Seeger, H., Tealeb, A., Toksöz, M. N., and Veis, G., 2000. Global positioning system constraints on plate kinematics and dynamics in the eastern Mediterranean and Caucasus, J. Geophys. Res., 105, 5695-5719.

Michael, A. J., 1984. Determination of stress from slip data: faults and folds. *J.* Geophys. Res., 89, 11,517–11,526.

Michael, A. J., 1987. Use of focal mechanisms to determine stress: a control study. J. Geophys. Res. 92, 357–368.

Michael, A. J., Ellsworth, W. L. and Oppenheimer, D., 1990. Co-seismic stress changes induced by the 1989 Loma Prieta, California earthquake. Geophys. Res. Lett. 17, 1441–1444.

Michael, A. J., 1991. Spatial variations of stress within the 1987 Whittier Narrows, California, aftershock sequence: new techniques and results. J. Geophys. Res. 96, 6303–6319.

Milkereit, C., Zunbul, S., Karakisa, S., Iravul, Y., Zschau, J., Baumbach, M., Grosser, H., Gunther, E., Umutlu, N., Kuru, T., Erkul, E., Klinge, K., Ibs von Seht, M., Karaman, A., 2000. Preliminary aftershock analysis of M_w=7.4 Izmit and M_w=7.1 Düzce earthquake in Western Turkey. In: Barka, A., Ö. Kozaci, S. Akyüz (Editors): The 1999 Izmit and Düzce Earthquakes: preliminary results. ISBN: 975-561-182-7, pp. 179-187, Istanbul Technical University.

Örgülü, G. and Aktar, M., 2001. Regional Moment Tensor Inversion for Strong Aftershocks of the August 17, 1999 Izmit Earthquake (Mw=7.4), Geophys. Res. Lett., 28(2), 371-374.

Peng, Z. and Ben-Zion, Y., 2004. Systematic analysis of crustal anisotropy along the Karadere-Düzce branch of the north Anatolian fault, Geophys. J. Int. 159, 253–274, doi: 10.1111/j.1365-246X. 2004.02379.x.

Pucci, S., Palyvos, N., Zabci, C., Pantosti, D. and Barchi, M., 2006. Coseismic ruptures and tectonic landforms along the Düzce segment of the North Anatolian Fault Zone (Ms 7.1, November 1999), J. Geophys. Res., 111, B06312, doi:10.1029/2004JB003578.

Reilinger, R., Ergintav, S., Bürgmann, R., McClusky, S., Lenk, O., Barka, A., Gurkan, O., Hearn, L., Feigl, K. L., Cakmak, R., Aktug, B., Ozener, H., Töksoz, M. N., 2000. Coesmic and postseismic fault slip for the 17 August 1999, M=7.5, Izmit, Turkey earthquake, Science, 289, 1519-1524.

Reilinger, R. McClusky, S., Vernant, P., Lawrence, S., Ergintav, S., Cakmak, R., Ozener, H., Kadirov, F., Guliev, I., Stepanyan, R., Nadariya, M., Hahubia, G., Mahmoud, S., Sakr, K., ArRajehi, A., Paradissis, D., Al-Aydrus, A., Prilepin, M., Guseva, T., Evren, E., Dmitrotsa, A., Filikov, S. V., Gomez, F., Al-Ghazzi, R., Karam, G., 2006. GPS constraints on continental deformation in the Africa-Arabia-Eurasia continental collision zone and implications for the dynamics of plate interactions, J. Geophys. Res., 111, B05411, doi:10.1029/2005JB004051.

Şaroğlu, F., Emre, Ö. and Kuşcu, I., 1992. *Active Fault Map of Turkey*, General Directorate of Mineral Research and Exploration (MTA), Eskisehir Yolu, 06520, Ankara, Turkey.

Seeber, L., Armbruster, J.G., Ozer, N., Aktar, M., Baris, S., Okaya, D., Ben-Zion,Y.& Field, E., 2000. The 1999 Earthquake Sequence along the North Anatolia Transform at the Juncture between the Two Main Ruptures, in The 1999 Izmit and Düzce Earthquakes: preliminary results, pp. 209–223, eds. Barka et al. Istanbul Technical University, Istanbul.

Snoke, J. A., 2003. FOCMEC: Focal mechanism determinations, in International Handbook of Earthquake and Engineering Seismology, edited by W. H. K. Lee et al., chap. 85.12, Academic, San Diego, Calif.

Tibi, R., Bock, G., Xia, Y., Baumbach, M., Grosser, H., Milkereit, C., Karakisa, S., Zunbul, S., Kind, R., Zschau, J., 2001. Rupture processes of the 1999 August 17 Izmit and November 12 Düzce (Turkey) earthquakes, Geophys. J. Int., 144, F1-F7.

Umutlu, N., Koketsu, K., Milkereit, C., 2004. The rupture process during the 1999 Düzce, Turkey, earthquake from joint inversion of teleseismic and strong-motion data, Tectonophysics, 391, 315-324.

Wessel, P., Smith, W.H.F., 1991. Free software helps map and display data. EOS, Trans., Am. Geophys. Union 72, 445–446.

Wiemer, S., 2001. A software package to analyze seismicity: ZMAP, Seis. Res. Lett., 72(2), 374-383.

Wiemer, S., Gerstenberger, M.C. and Hauksson, E., 2002. Properties of the 1999, Mw 7.1, Hector Mine earthquake: Implications for aftershock hazard, Bull. Seism. Soc. Am., 92, 1227-1240.

Wright, T., Fielding, E. and Parsons, B., 2001. Triggered slip: observations of the 17 August 1999 Izmit (Turkey) earthquake using radar interferometry, Geophys. Res. Lett., 28, 1079-1082.

Zoback, M. L., 1992. First and second order patterns of stress in the lithosphere: the world stress map project. J. Geophys. Res., 97, 11,703–11,728.

Figure Captions

Figure 1: a) Topographic map of the North Anatolian Fault Zone (NAFZ) region. Black arrows indicate the GPS-derived surface displacement rate (McClusky et al., 2000; Reilinger et al., 2006). **b)** Izmit-Düzce segment of the NAFZ. The Izmit-Düzce segment of the NAFZ is indicated by the rectangle and enlarged in Figure 3. Red lines indicate the Izmit 1999 surface rupture as mapped by Barka et al. (2002) and blue line indicates the Düzce 1999 surface rupture trace as mapped by Pucci et al. (2006). Hypocenters of the 1999 Izmit (blue) and Düzce (red) EQ are indicated by stars. Maximum surface displacement observed (5.2 m) is located east of Sapanca Lake. In the Izmit-Sapanca Lake segment, the maximum surface displacement observed is 3.5 m and in the Karadere segment 1.5 m. Colored circles represent Izmit aftershock epicenters along the rupture of the mainshock as recorded by the temporary seismic network (red triangles = stations of German Task-Force for Earthquakes network; yellow triangles = SABONET stations; see text for details. Event magnitudes are shown by different sized and colored circles. For reference, the Izmit M_w = 7.4 and the Düzce M_w = 7.2 strike-slip focal mechanisms are plotted (Tibi et. al, 2001).

Figure 2: Error distributions for Izmit aftershock fault plane solutions. The errors in given in degree for strike, dip and rake, respectively.

Figure 3: a) Karadere-Düzce branch of the NAFZ. Map view of the lower hemisphere projection of the 221 Izmit aftershock fault plane solutions analyzed in this study. Blue

ellipses indicate the Karadere Fault (KF) and Düzce Area (DA), respectively. **b)** Epicenters of the events shown in **(a)** scaled with magnitude. In addition, we plotted fault plane solutions of the early and M_l > 4.0 aftershocks (blue stars) (Örgülü and Aktar, 2001), the Izmit S1 subevent (M_w = 6.9, Tibi et al., 2001) and the Düzce mainshock (M_w = 7.2,) (black star) all reflecting an almost identical mechanism. Red and blue lines indicate the surface traces of the Karadere and Düzce Faults, respectively (Şaroğlu et al., 1992; Barka et al., 2002, Pucci et al., 2006) while the green area to the north of the Düzce Fault reflects the subsided Düzce Basin.

Figure 4: Representative examples of fault plane solutions from the Karadere-Düzce area (**a**-**d**). T and P indicate orientations of tension and pressure axes. Minus (dilatation) and plus (compression) signs indicate P wave polarity at the respective station.

Figure 5: Distribution of P (**a**) and T (**b**) axes for the 221 fault plane solutions determined in this study in equal-area projection of the lower hemispheres. The size of circles scales with magnitude and the shading indicates the source time (lighter color = later occurrence). P axes form a great circle trending NNW-SSE while T axes tend to cluster at shallow dip angle trending NE-SW. In total the data sets reflects dominantly strike-slip and normal faulting.

Figure 6: Distribution of P and T axes for the different subsets in equal-area lower hemisphere projection. The size of circles scales with magnitude and the shading indicates the hypocentral time (lighter color = later occurrence). **a)** 165 fault plane

solutions in the Düzce Area (DA). **b)** 56 fault plane solutions at the Karadere Fault (KF). **c)** 96 fault plane solutions at the northern DA (Düzce Basin). d) 69 fault plane solutions at the southern DA (Düzce Fault).

Figure 7: Stress field orientation as derived for the entire data set of fault 221 plane solutions. Black squares represent the 95% confidence region for maximum principle stress (σ_1 = S1= white square). Red triangles represent the 95% confidence region for the intermediate principal stress (σ_2 = S2 = white triangle). Blue circles represent the 95% confidence region for the minimum principle stress (σ_3 = S3 = white circle). Histogram of Φ values versus frequency is shown at the bottom. The $\overline{\beta}$ obtained for this inversion is 58° (see text for discussion).

Figure 8: a) Results of stress tensor inversion for 165 fault plane solutions at DA. **b)** 56 fault plane solutions at KF**. c)** 96 focal mechanisms at Düzce Basin. **d)** 69 focal mechanisms at the Düzce Fault. Symbols as in Figure 7. The $\overline{\beta}$ obtained for each inversion is plotted in the lower right of each subfigure (see text for discussion).

Figure 9: Results of stress tensor inversion for the two subvolumes within DA containing **a)** magnitudes $M_l > 2.0$ ($N = 53$); **b)** magnitudes $M_l < 2.0$ ($N = 112$). Results of stress tensor inversion for the two subvolumes within DA containing events at **c)** depths z > 10 km ($N = 104$) and **d)** depths z < 10 km ($N = 61$). The $\overline{\beta}$ obtained for each inversion is plotted in the lower right of each subfigure (see text for discussion).

Figure 10: Stress tensor inversion results for randomly selected subsets DA. High $\overline{\beta}$ obtained for each inversion is shown in the lower right of each subfigure. Stress tensor inversion results have poor fit.

Figure 11: a) Orientation of the trend of σ_1 (bars) within gridded subvolumes (1 km² with no depth limitation) smoothed over a 1 km radius of each node of the grid. Faulting regimes are represented by different colors as shown in the legend. The following abbreviations are used to describe the tectonic stress regime (Zoback, 1992): NF = Normal faulting, NS = Predominately normal faulting with strike-slip component, SS = Strike-Slip faulting, TS = Predominately thrust faulting with strike-slip component, TF = Thrust faulting. The black star displays the Düzce mainshock epicenter. **b)** Distribution of the variance of the stress tensor at each node as plotted in **(a)** according to Michael (1987). A high variance (> 0.2) indicates a strong heterogeneity of the stress field. The black star represents the Düzce mainshock epicenter.

Figure 12: Map of the lower hemisphere projection of the 221 Izmit aftershock fault plane solutions in Karadere Fault (KF) and Düzce Area (DA). Red and blue lines indicate the surface traces of the Karadere (KF) and Düzce (DF) Faults, respectively. The maximum coseismic Izmit surface displacement of the area is 1.5 m along the Karadere Fault. Surface displacement during the Düzce mainshock (12.11.1999 M_w = 7.2) in different sections of the Düzce Fault are also shown (0.5 m; 4 m; 5 m). Fault plane solutions of the early aftershocks (M_l > 4.0) (blue stars) (Örgülü and Aktar, 2001), the Izmit subevent (M_w = 6.9, Tibi et al., 2001) and the Düzce mainshock (black star) (M_w =

7.2) are reflecting an almost identical mechanism. The inset (**a**) in the above left shows the stress tensor inversion result for the Karadere Fault (KF). The inset (**b**) in the down left depicts surface map view of the *b*-value distribution and the depth distribution of *b*-values (Görgün et al., subm.). Numbers indicate coseismic slip for Izmit (red rectangle) and Düzce (blue rectangles) mainshocks along the Karadere and Düzce Faults, respectively. Red indicates the highest *b*-value (> 1.2) while blue reflects the lowest (≈ 0.7). White dots and big white star represent Izmit aftershocks and the Düzce mainshock, respectively. The inset (**c**) indicates the stress tensor inversion results for the Düzce Fault (southern DA) and Düzce Basin (northern DA). Results show that we have more strike-slip along the DF and more normal faulting at the DB in this study.

Table caption

Table 1: Results of stress tensor inversion for the entire set of 221 focal mechanisms at Karadere-Düzce Area (KDA) and for the seven subvolumes. DA, DB and DF represent Düzce Area, Düzce Basin and Düzce Fault, respectively. M1 and M2 refer to $M_l < 2.0$ and $M_l > 2.0$, respectively. D1 and D2 refer to z < 10 km and z > 10 km, respectively.

Figures

Figure 1:

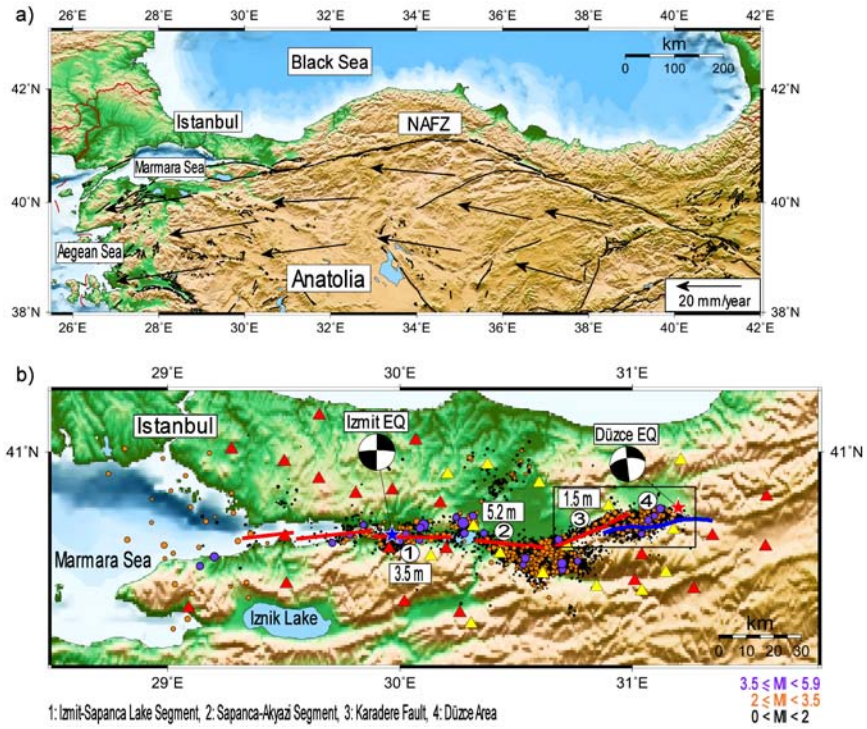

Figure 2:

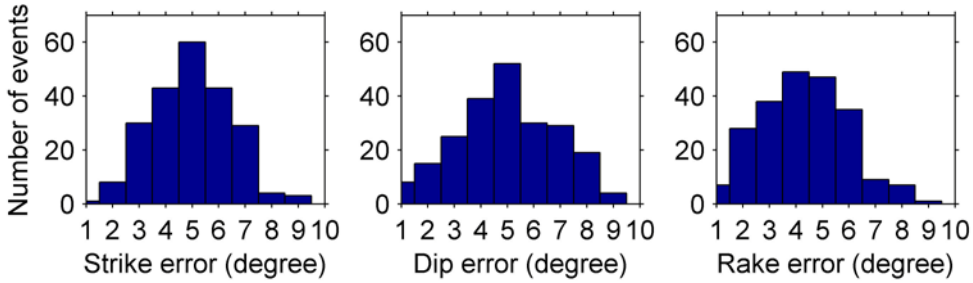

Figure 3:

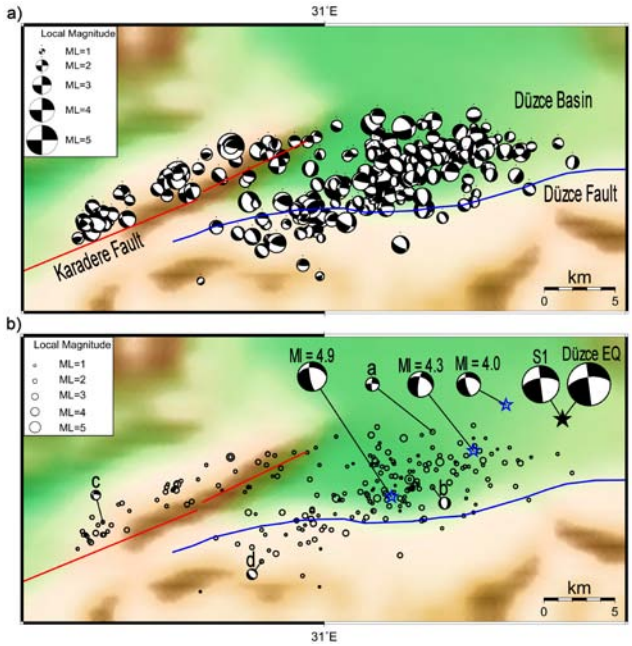

Figure 4:

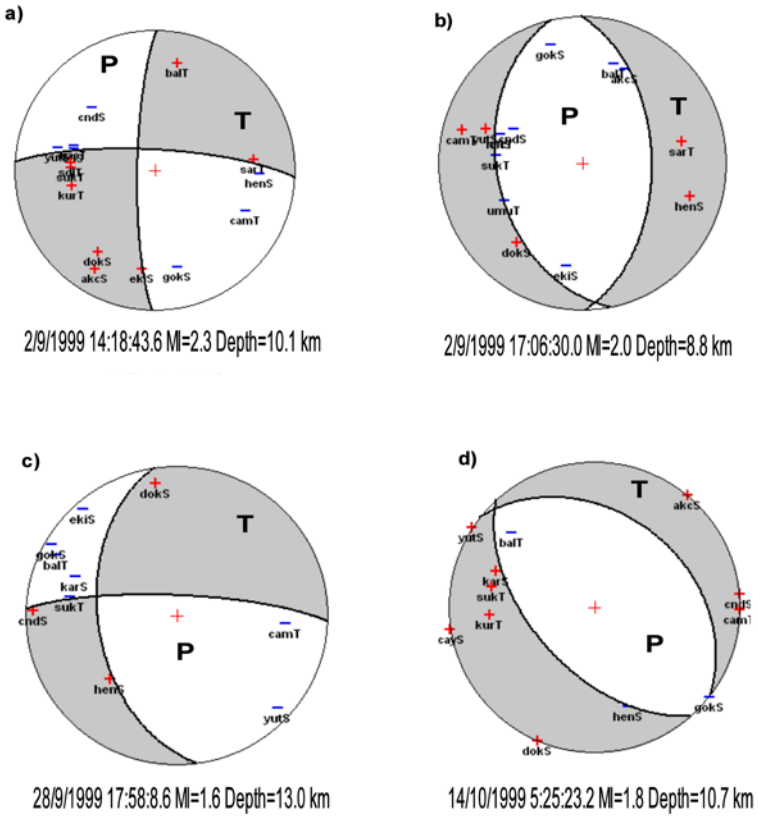

2/9/1999 14:18:43.6 Ml=2.3 Depth=10.1 km

2/9/1999 17:06:30.0 Ml=2.0 Depth=8.8 km

28/9/1999 17:58:8.6 Ml=1.6 Depth=13.0 km

14/10/1999 5:25:23.2 Ml=1.8 Depth=10.7 km

Figure 5:

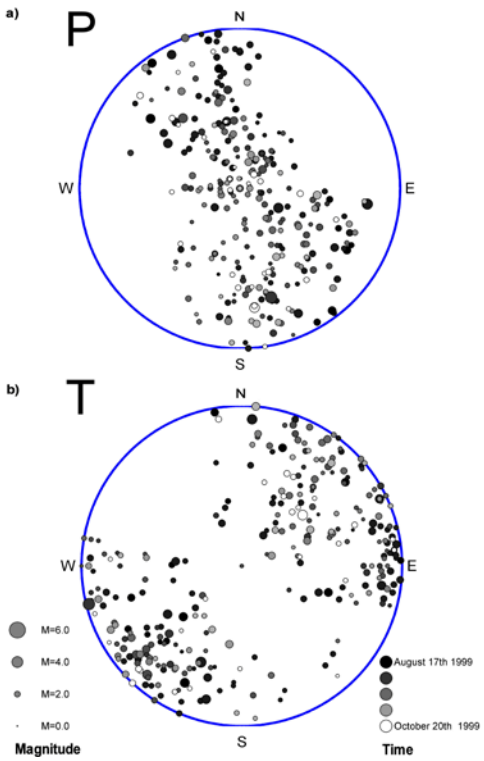

Figure 6:

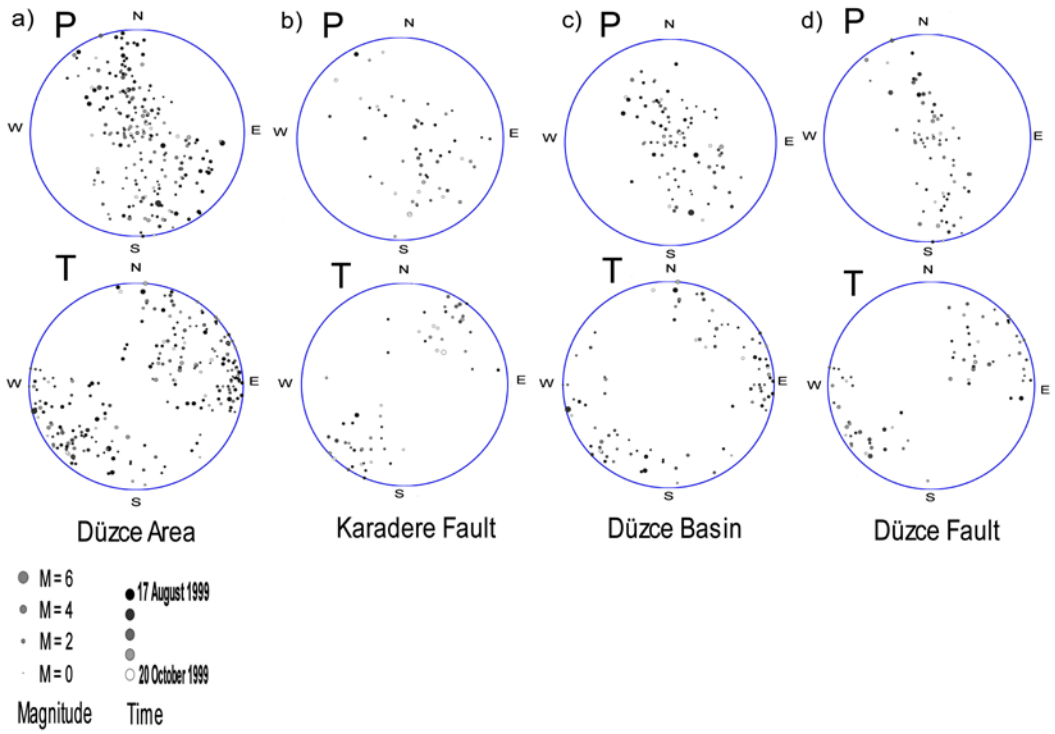

Figure 7:

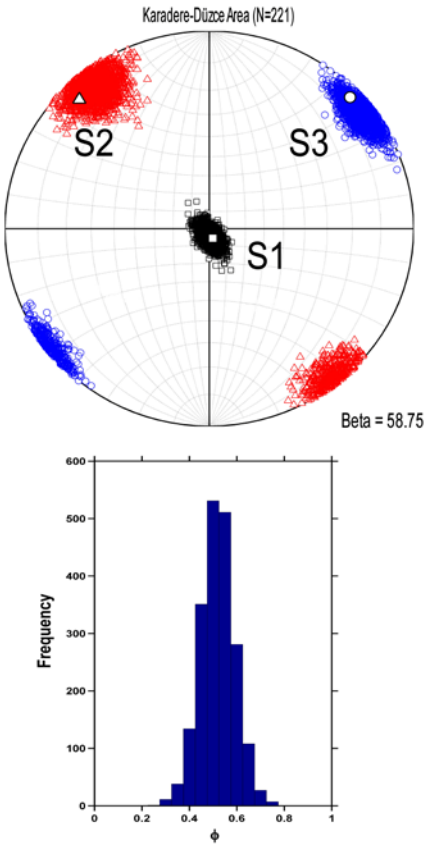

Figure 8:

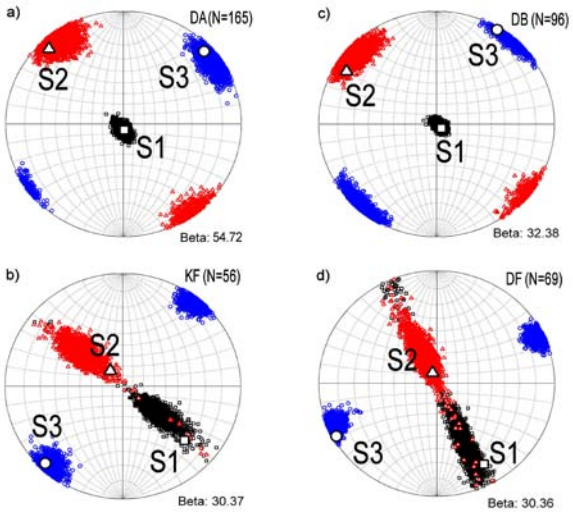

Figure 9:

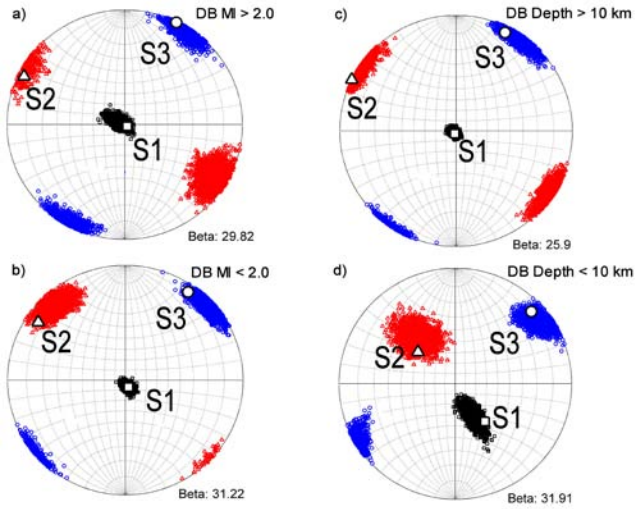

Figure 10:

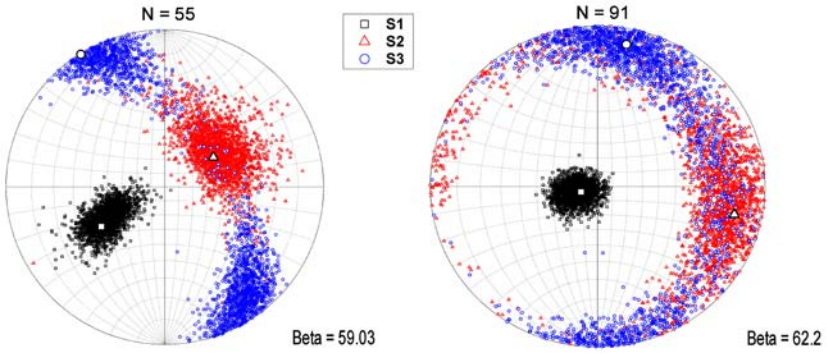

Figure 11:

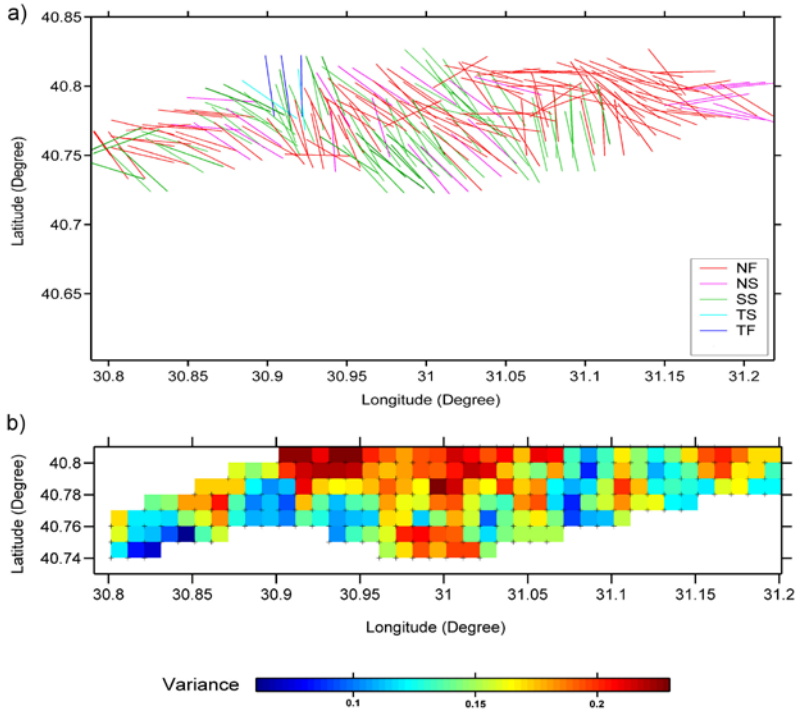

Figure 12: